

# Estimation of Surface Heat Flux in the Wind Tunnel Cascade Blades

J. Seume, A. Pourshaghaghay

*Space and time dependent heat flux on the surface of a blade mounted in the wind tunnel cascade is estimated by solving the inverse heat conduction problem (IHCP). The solution of the whole domain IHCP is carried out using two versions of the Variable Metric Method (VMM). These are the Symmetric Rank-one (SR1) and the Broydon–Fletcher–Goldfarb–Shanno (BFGS) versions. The objective is to evaluate the whole domain IHCP solution method based on VMM in the real experimental situations with complex geometries. The SR1 shows a little better performance than the BFGS. ANSYS software is utilized for the numerical solution of the direct heat conduction problem within the blade. The temperature data of sensors are acquired via an experiment on a heated blade encountering the cooling air flow inside a linear cascade wind tunnel.*

## 1 Introduction

The Inverse Heat Conduction Problem (IHCP) generally arises when the heat flux boundary condition on the surface of a body is not known a priori and is to be estimated using measured temperature data at several locations within or on the surface of the body. One of the solution methods of this type of IHCP is the whole domain approach which utilizes nonlinear optimization techniques as a tool to minimize a function of the sum of squares of errors (the objective function) and to find all unknown surface heat fluxes simultaneously. Depending on the type of the utilized optimization technique, the whole domain methodology may be called the conjugate gradient method (CGM), the Levenberg Marquardt method (LMM), or the Variable Metric Method (VMM, Quasi Newton Method). The CGM and LMM have been widely used in the field of IHCP. Comprehensive discussions of the CGM and the LMM are found in the text books by Ozicik and Orlande (2000) and the book by Alifanov (1994). There is a large number of papers that discuss the estimation of the unknown boundary conditions from the experimental measurement of temperatures. Some of these papers involve complex geometries. As a few examples, the articles by Kassab *et al.* (2001) in estimation of surface heat flux from liquid crystal thermography (LCT) temperature measurements, Louahlia-Gualous and Baonga (2008) in unsteady surface boundary conditions determination in impingement jet flow, Heng *et al.* (2010) in three dimensional transient nucleate boiling heat flux over thin heating foil, Das *et al.* (2005) in estimation of the local Nusselt number distribution over a flat and a ribbed surface from LCT measurements, Gardarein *et al.* (2009) in 2D heat flux calculations using both infrared and thermocouple measurement systems, Nallathambi and Specht (2008) in heat flux prediction in the metal quenching process by array of jets, Huang *et al.* (2007) in three-dimensional inverse heat flux calculations on the drilling surface of a drilling tool can be quoted. In a recent paper that has some similarities to our work, Chen and Yang (2008) estimated the inlet temperature of flow over the two dimensional rectangular blade using the CGM.

The VMM is relatively new among the whole domain IHCP solution methods. Kowsary *et al.* (2006) and Pourshaghaghay *et al.* (2007) applied VMM to solve one and two dimensional IHCPs. There are several versions of the VMM in the literature. Lukšan and Spedicato (2000) theoretically reviewed different VMM's in general unconstrained optimization problems. In the present study, the Broydon–Fletcher–Goldfarb–Shanno (BFGS) and the Symmetric Rank-one (SR1) methods are examined in the complex geometry of a two dimensional straight turbine blade using empirical thermocouple data. As mentioned above, there are a number

of papers that use empirical sensor data in the different inverse heat transfer problems. Nonetheless, there is no published work utilizing empirical thermocouple data for IHCP calculations over a turbine blade surface.

Any IHCP code has a subroutine in order to solve the direct heat conduction problem for given or arbitrary values of the boundary conditions. This subroutine is called many times by the main code during the runtime of the IHCP algorithm. When the body has a complex geometry like a blade profile, the calculation of the direct unsteady heat conduction equation inside the body is a difficult issue. One approach in such complex geometries is to write the whole IHCP code in the ANSYS Parametric Design Language (APDL) of the ANSYS classic software. Using APDL, one is able to employ ANSYS in order to set and change the boundary conditions over the geometry, pass the solution of the direct heat problem to the software, and then recall the direct solution many times during the IHCP calculations. This approach is taken in this work, and all programmes in the present work are written with APDL in ANSYS classic version 12. A list of APDL commands and some comments on the macro writing in this language are found in the software manual.

## 2 The Experimental Facility

The considered straight turbine blade has a two-dimensional geometry and is made of steel X20Cr13 with the properties of  $c_p = 460 \text{ J/kg.K}$ ,  $\rho = 7750 \text{ kg/m}^3$ , and  $k = 25 \text{ W/m.K}$ . Two photos of such blades are shown in Figure 1. They are model blades, the original use of which is to study the effect of the blade surface roughness on the air flow in wind tunnel. Every blade has a mounting block on each end to fix the blade to the side walls of the cascade wind tunnel. The profile of the blade is uniform over its span. Hence, a two dimensional heat conduction equation can be considered at the mid section of the blade due to its symmetry if one wants to solve the heat conduction problem in the middle of blade span. The blade has a span of  $240 \text{ mm}$  and a chord length of  $c = 73 \text{ mm}$ . Some blades will be equipped with electric heaters which are placed inside the blades. For numerical calculations, it is required to know the profile of the cross section of the blade. Thus, the coordinates  $(x, y)$  of 160 points on the surface of the blade are measured. Figure 2 shows the depicted profile of the blade based on these points. The cylindrical hole inside the blade is made in order to insert the electric heater. The wind tunnel cascade has seven neighboring positions in which seven blades can be put as shown in Figure 3, with a pitch value of  $p = 57.3 \text{ mm}$ , and a staggering angle  $\gamma = 49^\circ$ . The cascade itself is placed in the wind tunnel. The cross section of wind tunnel has the dimensions of  $240 \text{ mm} \times 408 \text{ mm}$ . The only adjustable parameter in the current cascade wind tunnel is the incoming mass flow rate. The inlet temperature  $T$ , the inlet static pressure  $P$ , and the inlet total pressure  $P_0$  are measured in the upstream of the cascade in the wind tunnel.

Three central adjacent blades in the cascade are perforated so that three electric heaters with identical power can be placed inside them. Hence, a complete periodic conditions is provided for the middle blade in which the



Figure 1: Two images of the straight turbine blade

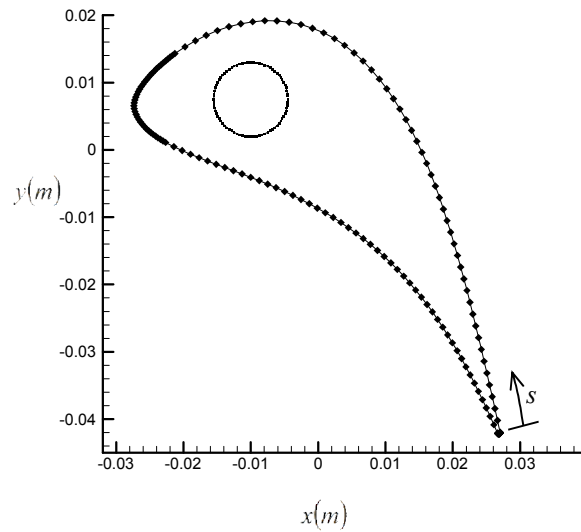


Figure 2: The cross section profile of the blade. The coordinates are measured at the points which are shown as the filled dotted points.  $s$  is the arc length along the outer surface starting from trailing edge.

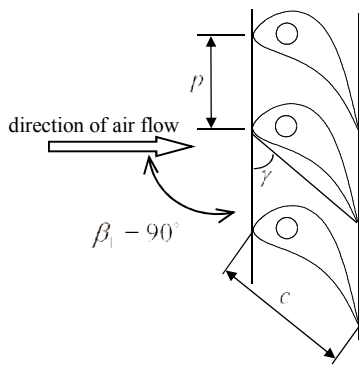


Figure 3: Turbine blade cascade

measurements of temperature are carried out. Each heater with the length of  $240\text{ mm}$  and the diameter of  $10\text{ mm}$  generates  $1500\text{ W}$  thermal energy rate. As soon as the air flow at ambient temperature supplied by the wind tunnel passes through the blades with turned-on heaters, the convective heat transfer starts on the surface of the blades. If the time is allowed to pass enough, a steady-state condition will be reached. Afterwards, the heaters are turned off while the air flow continues to pass through the blades. Since there is no input energy to the blades in this state, the heat transfer from the surface becomes transient. The aim is to estimate the surface heat flux during a range of time in this transient state using the temperatures measured by several thermocouples.

The thermocouples have  $0.5\text{ mm}$  diameter. A number of grooves with a depth of  $0.7\text{ mm}$  are made on the blade surface from one edge of the blade to the one-half of its span length so that the thermocouple wires can be embedded within them. The tip of thermocouples is in the middle of the blade span. Then the grooves, except near mid-span section, are filled with glue so that the surface remains smooth. The wires of thermocouples exit from the holes made in the side block of the blade and are connected to the data acquisition system. The LabVIEW software is used for monitoring, data acquisition, and for storing the data.

### 3 The Inverse Formulation

We consider the following heat conduction equation at the mid-span cross section of the blade cooled by air:

$$\frac{\partial^2 T}{\partial x^2} + \frac{\partial^2 T}{\partial y^2} = \frac{1}{\alpha} \frac{\partial T}{\partial t} \quad (1-a)$$

$$-k \frac{\partial T}{\partial \bar{n}} = q(x, y, t) \text{ on the outer surface of the blade} \quad (1-b)$$

$$\frac{\partial T}{\partial \bar{n}} = 0 \text{ on the surface of the inner circle} \quad (1-c)$$

$$T(t = 0) = T_0(x, y) \quad (1-d)$$

The initial condition  $T_0(x, y)$  is the temperature field within the blade just after turning off the heaters. This temperature does not have a uniform distribution. This temperature distribution is not known a priori but must be found via the simulation of the air flow over the blade in the wind tunnel which is carried out in this work using the FLOTTRAN module of ANSYS software. Through this simulation, first a heat flux proportional to the power of the heater is applied on the surface of the circle inside the blade. Subsequently, a steady state solution for the temperature fields of the fluid and the blade is calculated in ANSYS. Then the temperature value of each node inside the blade is captured by APDL commands and is saved into a file as  $T_0$  in that node. Accordingly,  $t$  in equations (1) is the time after turning off the heater. In order to find the unknown heat flux  $q(x, y, t)$ , the outer surface of the blade is supposed to be divided into a number of sections (Figure 4). In each section, a uniform heat flux is exposed as observed in Figure 4. Each of these spatial components of heat flux will be called  $q^{\bar{n}}(t)$  where  $\bar{n} = 1, 2, \dots, n_s$ . We chose nine sections along the blade surface ( $n_s = 9$ ) for the heat flux considering a compromise between exactness and computational time. Each  $q^{\bar{n}}(t)$  is separately discretized into a number of sub-components over the total time period. The total range of time in the problem consists of  $M$  time steps. The sensors save the temperature in each of these time steps. As some inaccuracies usually appear in the solutions of IHCP near final times, the total number of sensor time steps  $M$  is divided into  $M_1 + M_2$  time steps where  $M_2$  is much less than  $M_1$ . The heat flux is estimated for the  $M_1$  time steps using all  $M_1 + M_2$  data points of each sensor.

A single vector of unknowns  $\vec{q}$  can be formed in order to gather all of the heat flux components as

$$\vec{q}_{n \times 1} = [q^1(t_1) \quad q^1(t_2) \quad \dots \quad q^1(t_{M_1}) \quad q^2(t_1) \quad q^2(t_2) \quad \dots \quad q^2(t_{M_1}) \quad \dots] = [q_1^1 \quad q_2^1 \quad \dots \quad q_{M_1}^1 \quad q_1^2 \quad q_2^2 \quad \dots \quad q_{M_1}^2 \quad \dots] \quad (2)$$

$n$  is total number of unknowns, equal to  $n_s \times M_1$ . The function of sum of square errors is then defined as

$$f = \sum_{k=1}^K \sum_{m=1}^M [Y(x_k, y_k, t_m) - T(x_k, y_k, t_m, \vec{q})]^2 \quad (3)$$

in which  $K$  is the total number of applied sensors,  $Y$  is the measured temperature at the location of sensor  $k^{th}$ , and  $T$  is the calculated temperature utilizing a direct heat conduction model (equation (1)) based on a given or assumed vector of  $\vec{q}$ . The unknown vector  $\vec{q}$  should be searched for such that it minimizes the objective function  $f$  in equation (3). The VMM is used here to find the minimum point of the function  $f$ . The detailed formulation of the VMM including BFGS and SR1 updating formulas as well as the definition of pulse sensitivity coefficients are found in the papers by Kowsary *et al.* and Pourshaghaghay *et al.* In order to find the optimal step length  $\lambda_i^*$  in the search direction  $\vec{S}_i$  in iteration cycle  $i^{th}$  of the VMM, the following equation is used

$$\lambda_i^* = \frac{\sum_{k=1}^K \sum_{m=1}^M \left\{ [Y(x_k, t_m) - T(x_k, t_m, \bar{q}_i)] \left[ \sum_{\tilde{m}=1}^{M_1} \sum_{\tilde{n}=1}^{n_s} X(x_k, t_m, q_{\tilde{m}}^{\tilde{n}}) \times S_{(\tilde{n}-1) \times M_1 + \tilde{m}} \right] \right\}}{\sum_{k=1}^K \sum_{m=1}^M \left[ \left( \sum_{\tilde{m}=1}^{M_1} \sum_{\tilde{n}=1}^{n_s} X(x_k, t_m, q_{\tilde{m}}^{\tilde{n}}) \times S_{(\tilde{n}-1) \times M_1 + \tilde{m}} \right)^2 \right]} \quad (4)$$

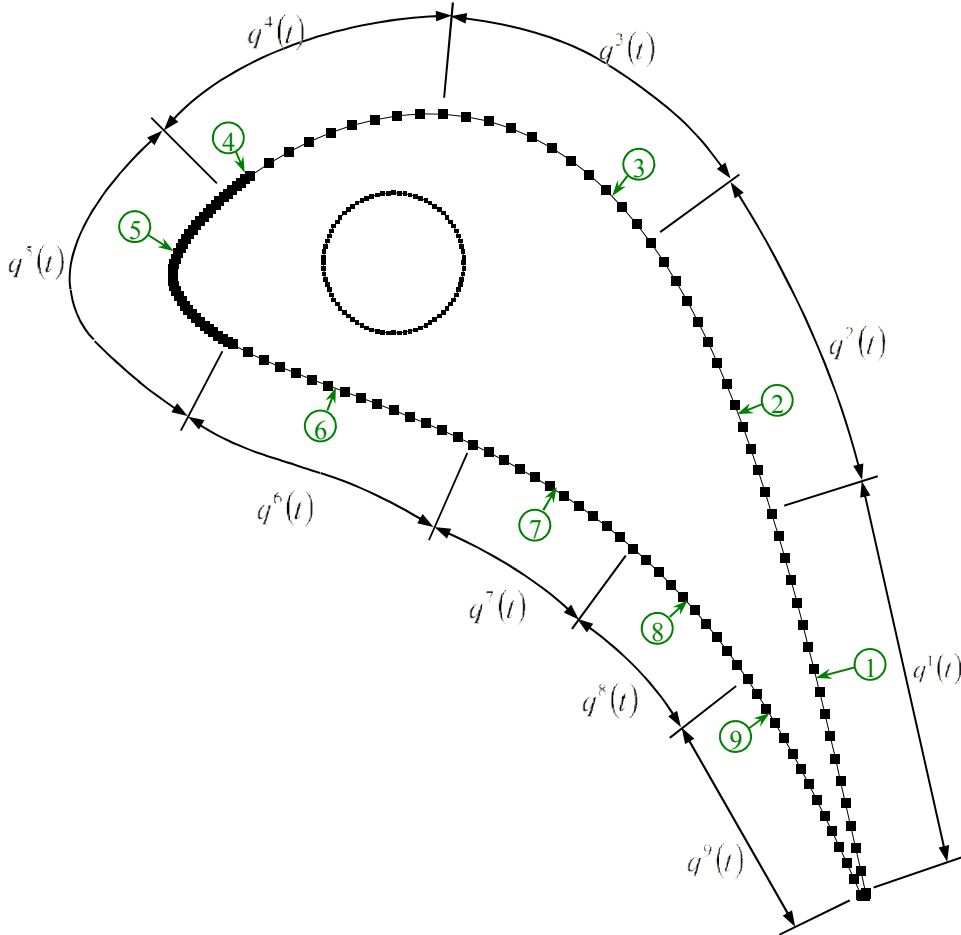


Figure 4: Dividing of heat flux over the blade surface into nine uniform spatial components. Numbers 1 to 9 inside the circles show the locations of nine sensors on the surface.

#### 4 Computational Domains and Numerical Approach

Figure 5 depicts the computational domain used in ANSYS in order to solve fluid flow and conjugate heat transfer over the middle blade in the turbine cascade of Figure 3. The domain in Figure 5 is used for simulating the flow in the wind tunnel in order to design and to model the experiment, to calculate the temperature distribution inside the blade as an initial condition for the IHCP code, and to generate sensor data to be used in the validation of the inverse code. Another domain containing only the blade geometry is formed in which the IHCP code written in APDL is run. The distance between the upper and lower boundary lines in Figure 5 is equal to the pitch value  $p = 57.3 \text{ mm}$ . The FLOTTRAN module of the software (using element type of fluid141) is utilized to solve the momentum and the energy equations. This element type in triangular form with refinement around the surface is used both in fluid and solid regions which contain in all nearly  $2.5 \times 10^5$  nodes. In the other domain containing only the blade, the number of nodes is nearly  $5.6 \times 10^4$ . In this second domain, the IHCP (APDL) code is run using element type plane55 and the thermal module of the software.

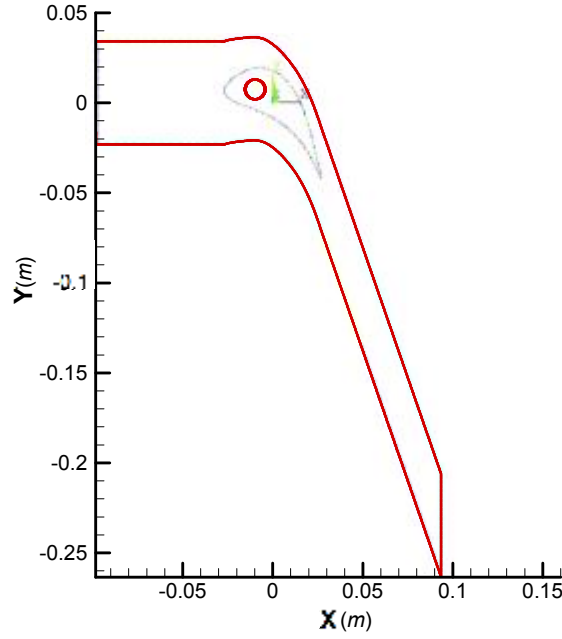


Figure 5: Computational domain formed in ANSYS to simulate the flow in wind tunnel

The shear stress transport SST turbulence model along with the spalding near-wall treatment is chosen in the software for modeling of turbulence. A time step of  $0.1\text{sec}$  is used for all numerical calculations. This time step is not equal to the sensor time step for saving temperature data. In order to solve the problem of the conjugate heat transfer in the wind tunnel flow simulation with the FLOTRAN module, the velocity is set equal to zero in the area that contains the solid blade. Moreover, the material properties ( $\rho, c_p, k$ ) of the solid are defined for this area instead of air properties. Within this approach, temperature continuity and heat flux conservation are automatically fulfilled at the interface between the blade and the air flow.

Below, first the results for the verification of the written IHCP codes are presented. This is performed utilizing only simulated sensor temperatures and simulated wind tunnel flow. Subsequently, the estimated results from the experimental temperatures are presented.

## 5 Verification of Flow Calculation

The following boundary conditions are applied to the geometry of Figure 5:  $25\text{ m/s}$  for  $x$ -component of velocity and  $297\text{K}$  as the temperature of the inlet boundary, zero relative pressure at the outlet, a value of  $199\text{ kW/m}^2$  as the heat flux on the surface of the inner circle (corresponding to the power of actual applied heaters  $1.5\text{ kW}$ ), and periodic boundary conditions for upper and lower boundary lines using command PERI of APDL. The inlet turbulence intensity of the cascade wind tunnel is increased to 4% by a rather coarse turbulence grid located about  $2\text{ m}$  in upstream of the cascade. Hence, the turbulent kinetic energy ( $\kappa_{in}$ ) and the turbulent energy dissipation rate ( $\epsilon_{in}$ ) are also applied as 1.5 and 22, respectively, at inlet boundary based on the following equations (manual of ANSYS-CFX 12)

$$\kappa_{in} = 1.5(0.04U_{in})^2 \quad (5)$$

$$\epsilon_{in} = \kappa_{in}^{1.5} / (l_t) \quad (6)$$

in which  $l_t$  is the inlet turbulent length scale equal to  $83\text{ mm}$ .

A steady state flow solution is presented in Figure 6 for the pressure, the velocity, and the temperature fields. The resulting temperature field inside the blade is saved as an initial condition of equations (1) in order to be used later in the inverse code.

In Table 1, the convective heat transfer coefficient ( $h$ ) at the point of sensor 5, recovered directly by the software after flow simulation, is compared with some reported empirical data for this parameter in the cascade turbine blade. Although these experimental data correspond to different turbine blade geometries, the leading edge contours of these blades can be approximated to the current blade contour very near to stagnation point. Therefore, the values of convection coefficient given by these references near the stagnation point on the suction side can be compared to the current results to verify the numerical calculations of flow field. The grid independency is also shown in this table for the nodes number of  $2.5 \times 10^5$ .

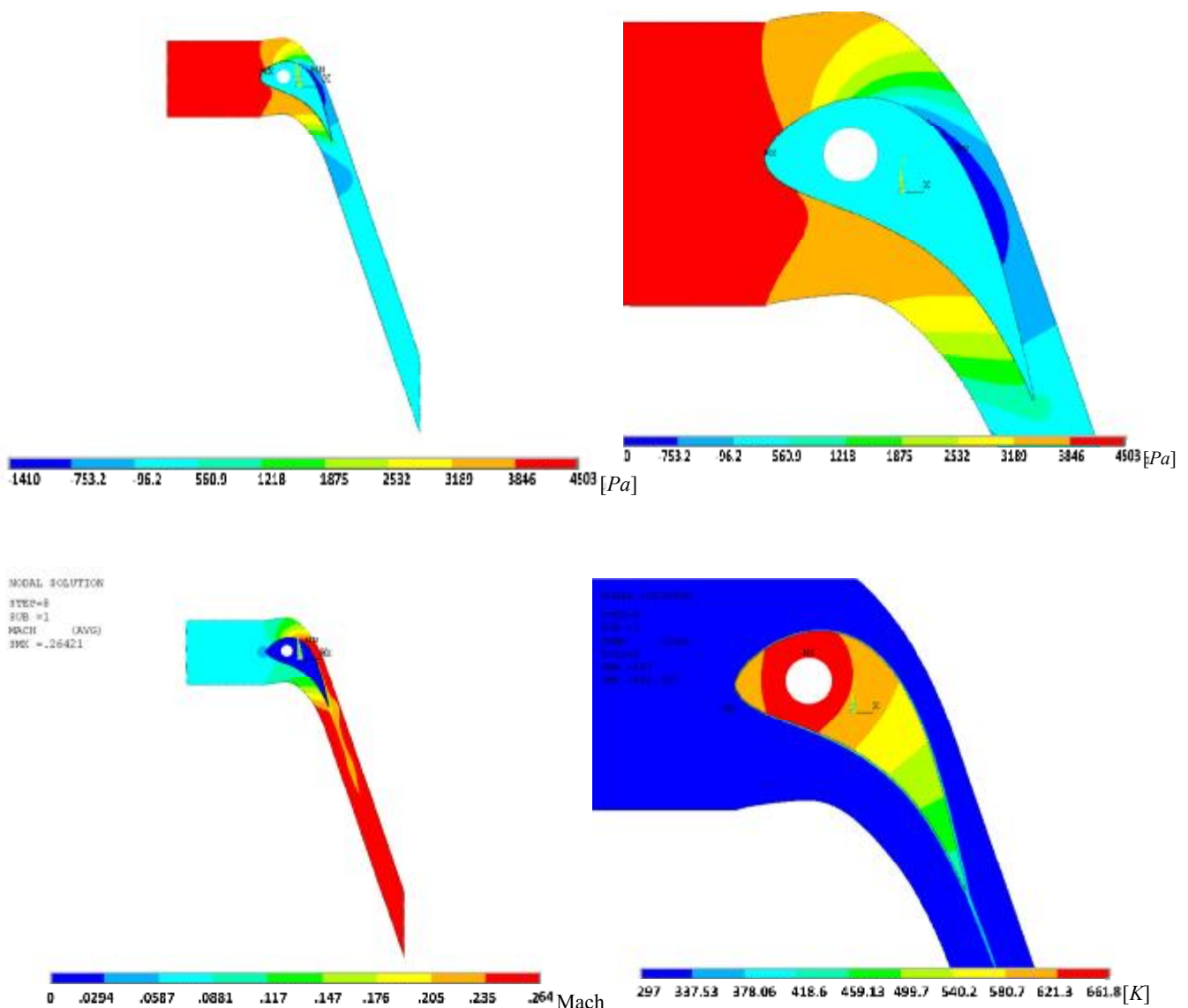


Figure 6: The steady state results of the flow simulation for (from top to down) relative pressure, Mach number, and temperature fields

Table 1: The values of local convection coefficient at the position of sensor 5,  $Re_c=1.22E3$

	Convection coefficient[W/m <sup>2</sup> K]
ANSYS modelling Number of nodes: $2.29 \times 10^5$	371.5
ANSYS modelling Number of nodes: $2.5 \times 10^5$	372.1
ANSYS modelling Number of nodes: $3.66 \times 10^5$	373
Byvaltsev and Nagashima (1998) (Figure 9) also cited by Chen and Yang (2008)	$\approx 357$
Butler <i>et al.</i> (2001) (Figure 7)	$\approx 380-385$
Choi <i>et al.</i> (2004) (Figures 7 and 8)	$\approx 475$

## 6 Verification of the IHCP code

After obtaining the steady state solution (Figure 6) related to turned-on heaters; zero heat flux corresponding to the turned-off heaters is prescribed on the inner circle of the blade, and FLOTRAN is run in the transient mode for solving the energy equation while the flow solver is off. During this stage of simulation, the temperature values of several locations on the surface of the blade are saved as thermocouple data. After some numerical trials and attempts in reaching appropriate IHCP results and keeping the computational time and computer memory low, nine locations on the surface of the blade (shown in Figure 4) are chosen at which temperature values are saved in every 0.5sec. These locations are specified in Figure 4 by the arrows numbered from 1 to 9. The heat flux values at the lines forming the blade surface are captured and are averaged over each nine sections of Figure 4 in order to be compared with the heat flux estimated by IHCP. In fact, these heat fluxes are flux distribution over the blade surface resulted from numerical simulation of wind tunnel flow.

Figure 7 displays nine spatial heat fluxes estimated from simulated sensor data without noise versus the surface heat flux resulted from numerical simulation of wind tunnel flow. The estimated heat flux and the simulated heat flux in this figure are related to two different domains in ANSYS, one used in air flow simulation and one used in IHCP calculations containing only the blade. The maximum number of 30 iterations is considered as a stopping criterion of VMM iterations. The relative difference between the estimated heat flux vector  $\vec{q}$  and those acquired by the software simulation can be defined as

$$e = \left( \sqrt{\sum_{n=1}^{n_s} \sum_{m=1}^{M_1} (q_{m,Est.}^n - q_{m,simulation}^n)^2} \right) / \left( \sqrt{\sum_{n=1}^{n_s} \sum_{m=1}^{M_1} (q_{m,simulation}^n)^2} \right) \quad (7)$$

This relative difference is 6.45% for BFGS and 6.43% for SR1 for the case shown in Figure 7. The reasons for this relative difference are first that the heat flux in direct flow simulation is continuous along the boundary while it is discrete in the inverse problem. There is indeed the limitation of using only few discrete spatial heat flux components which limits the resolution of the inverse method. Another reason for this difference is that different solvers with different element types and mesh domains are used in direct heat flux (flow simulation) and IHCP calculations. As it is usual in the IHCP studies, the sensor data are then made noisy using an additive error term as

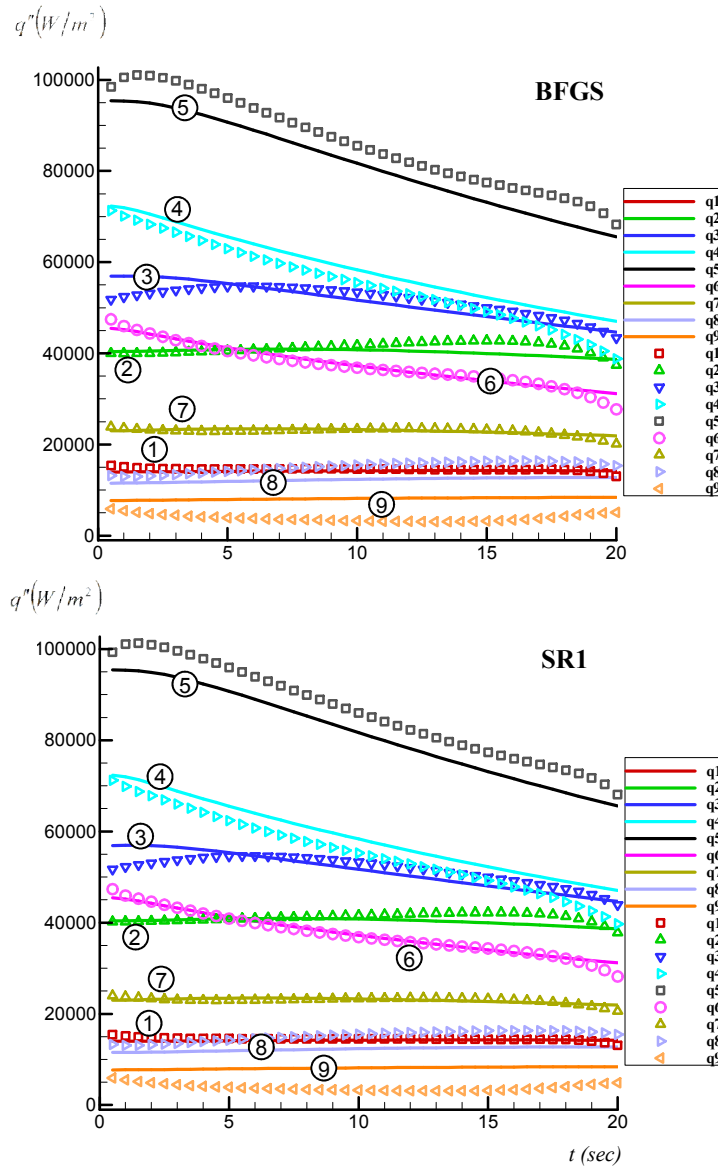


Figure 7: Nine spatial components of surface heat flux (specified by numbers 1 to 9 inside the circles) estimated from simulated sensor data without noise, for BFGS and SR1 versions. The symbols are the VMM results, and the lines are heat fluxes directly acquired from the wind tunnel simulation in the software.

$$Y_{noisy} = Y + \omega\sigma \quad (8)$$

where  $\omega$  is a random variable with normal distribution and zero mean and unitary standard deviation; and  $\sigma$  is the standard deviation of the measurement errors which is chosen equal to 1.5K. The estimated heat fluxes based on noisy sensor data are depicted in Figure 8. The relative difference  $e$  is 9.57% for BFGS and 9.46% for SR1. The results of estimation in Figures 7 and 8 are able to validate the IHCP code.

## 7 Results

### 7.1. Operating conditions

A digital controller should be utilized to raise the temperature of heaters slowly; otherwise the heaters may be

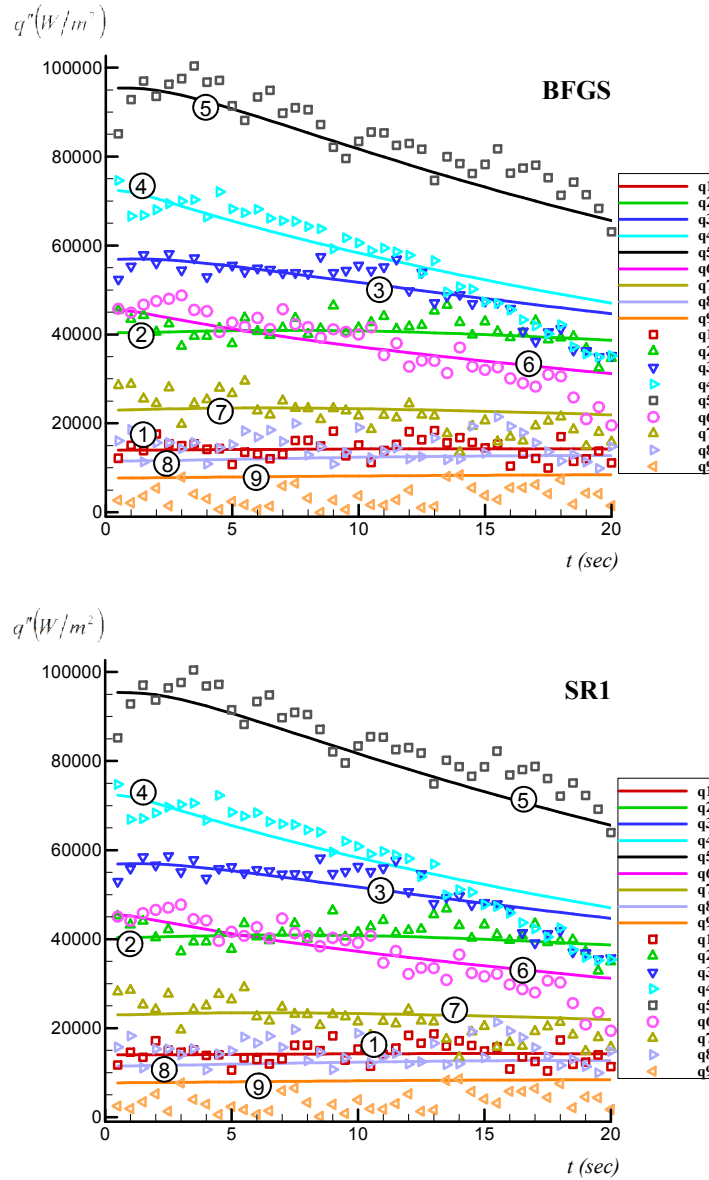


Figure 8: The estimated surface heat flux using noisy simulated sensor data, for BFGS and SR1 versions. The symbols are the VMM results, and the lines are the results of the wind tunnel simulation. Numbers 1 to 9 inside the circles specify number of spatial heat flux components.

burnt. For this reason, one heater is equipped with an inner thermocouple which sends the temperature value inside the heater to the controller. When this temperature raises over the set point temperature (chosen as  $470 \pm 3^\circ\text{C}$ ), the controller turns off three heaters until the heat transfer to the fluid causes the heater's temperature to be reduced lower than the set point. Then the heaters are again turns on by the controller. Under these conditions for the power of heaters which is shown in Figure 9, a truly complete steady state can not be acquired. Instead, a periodic steady state conditions can be reached in which the observed oscillations in the monitored temperature at sensor locations are around one degree. Three heaters are then shut down completely and sensor temperatures are immediately saved for a while to be used later.

## 7.2. Source of the experimental and the modeling uncertainty

The inlet temperature cannot be controlled and is a function of environmental conditions. In the three experiments carried out, it was  $14.1^\circ\text{C}$ ,  $17^\circ\text{C}$ , and  $17^\circ\text{C}$ . As the velocity magnitude of  $25\text{ m/s}$  is desired at the inlet, a Mach number equal to 0.073 should be imposed at the inlet by changing the incoming mass flow rate. There are some oscillations in Mach number value at the inlet (around  $\pm 0.001$ ) due to the noise in parameters

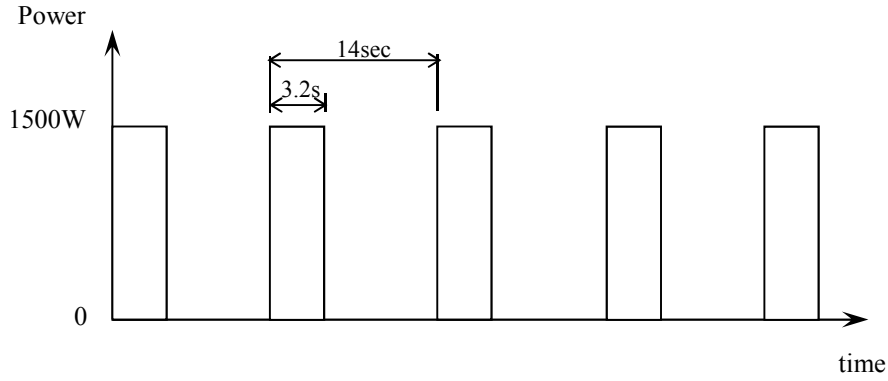


Figure 9: The power of cartridge heaters as a function of time during the experiment

such as compressor speed and inlet pressure. The L-curve method (Alifanov (1994)) is used as the stopping criterion in which VMM iterations are cut at the cross section of two lines forming the “L” curve in the objective function reduction history.

In the current IHCP, another source of errors also exists that is related to the initial temperature field within the blade just after shutting down the heaters. This temperature distribution has considerable effects on the IHCP results near  $t = 0$  when it is used as the initial condition of heat conduction equation in the VMM calculations. Since this temperature field at the beginning of the IHCP experiment is found numerically, the difference between the numerical and the actual temperatures affects the estimated results due to the ill-posed nature of IHCP. This temperature is calculated by repeating the simulation of flow in ANSYS applying the heat flux of Figure 9 on the inner circle within the blade.

The examination of simulated temperatures at sensor locations in different software runs revealed that the type of turbulence model and appropriate values for its parameters affects the accuracy of the calculated flow field. The value of turbulent Prandtl-Schmidt number for the energy equation ( $\sigma_t$ ) has significant effect on the predicted temperature field of the conjugate heat transfer problem in the ANSYS software. The turbulent contribution to the diffusion term of the energy equation is divided by this parameter (manual of ANSYS 12).

### 7.3. Simulation versus experimental data

Using the default value of parameter  $\sigma_t = 0.85$ , ANSYS yields the temperature results which are different from experimental sensor data. In Table 2, the temperatures of nine sensors saved in the experiment just after complete turning off the heaters are compared with the temperatures at sensor locations computed by the software. It is observed that the numerical values corresponding to  $\sigma_t = 0.85$  are lower than the experimental ones. Increasing the value of parameter  $\sigma_t$  causes the calculated temperature by the software inside the blade to rise. This is interpreted using the definition of  $\sigma_t$  which is the ratio of eddy viscosity to eddy conductivity. Increasing the value of  $\sigma_t$  means eddy conductivity of turbulence flow is reduced. Thus the heat transfer to the fluid is reduced, and this leads to rising temperature of the blade and sensors. After several trials, the optimal value turned out to be  $\sigma_t = 5.7$  along with applying “Spalding near wall treatment” and the shear stress transport SST turbulent model. Though, there is still considerable difference between simulated and real data for sensor 5. Such differences would also exist in temperature values of the region inside the blade near stagnation point and location 5 that would affect IHCP result when they are used as initial condition of the heat equation. The results of Figure 6 are also based on  $\sigma_t = 5.7$ . It is seen from Table 2, a small value of  $\sigma_t$  is appropriate for flow around stagnation point while greater values are needed for the flow in other regions.

The examination of the fluid temperature very near to the solid surface is interesting. Figure 10 shows numerical values of the temperature at the start of the transient duration around sensors 5 and 3. It is observed that the temperature in the first grid in fluid just adjacent to the interface falls considerably. It is notable that the

length between the first grid in fluid and the solid surface grid in Figure 10-a is  $2.5 \times 10^{-2}mm$ . This shows that the errors will occur in sensing the solid temperature if the tip of thermocouple is laid slightly in fluid region.

Table 2: Temperature values (K) at sensor locations just after complete turning off the heaters

Sensor Number	Experiment	Simulation, $\sigma_t = 0.85$	Simulation, $\sigma_t = 5.7$
1	334.72	314.98	338.71
2	357.75	329.17	356.74
3	368.90	338.87	370.08
4	373.09	347.85	376.16
5	343.84	341.94	369.41
6	377.70	355.77	381.17
7	364.20	334.95	362.90
8	348.61	321.36	348.18
9	334.35	311.67	337.70

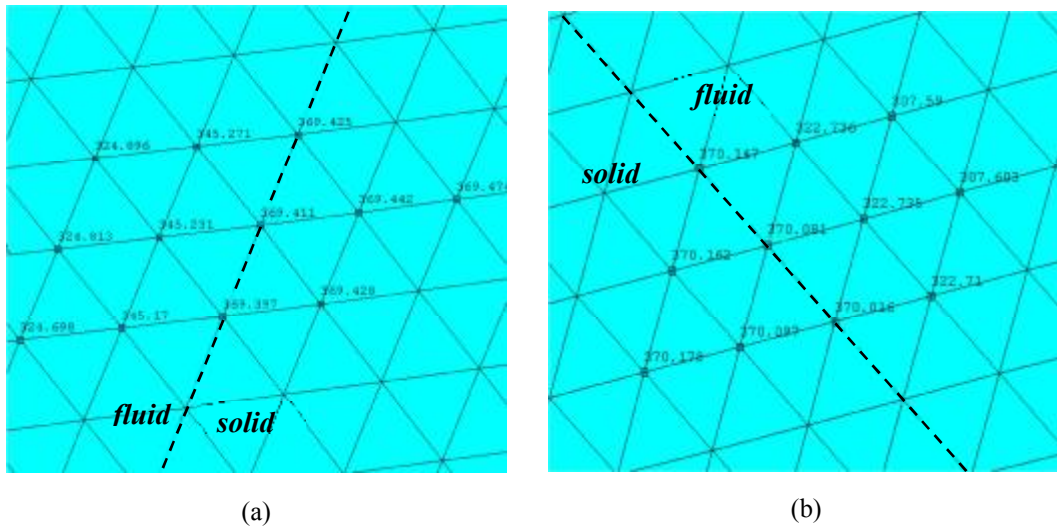


Figure 10: Temperature of nodes around the position of sensors at the interface surface.  
(a) sensor 5, (b) sensor 3

Due to the difference between the data of sensor 5 and the simulated temperature inside the blade around this region, the estimated heat flux components deviates largely from simulated results. In order to obtain an elegant flux estimation, local convection coefficient ( $h$ ) at the position of sensor 5 based on an experimental correlation (taken from Figure 7 of the paper by Butler *et al.* (2001)) as well as local heat flux at this position taken from software simulation are replaced in the following relation

$$q(t) = h_5(T_5(t) - T_\infty) \quad (9)$$

Next,  $T_5(t)$  is calculated and replaced for data of sensor 5. The estimated heat fluxes based on these set of data are plotted in Figure 11. The difference between the estimated heat flux vector and the software predicted vector is 36.5% for BFGS and is 35.5% for SR1. Maximum heat transfer from blade to fluid occurs near the

stagnation point, i.e. in region 5, as it is expected. The next highest heat transfers occur in the suction side of blade in regions 4 and 3.

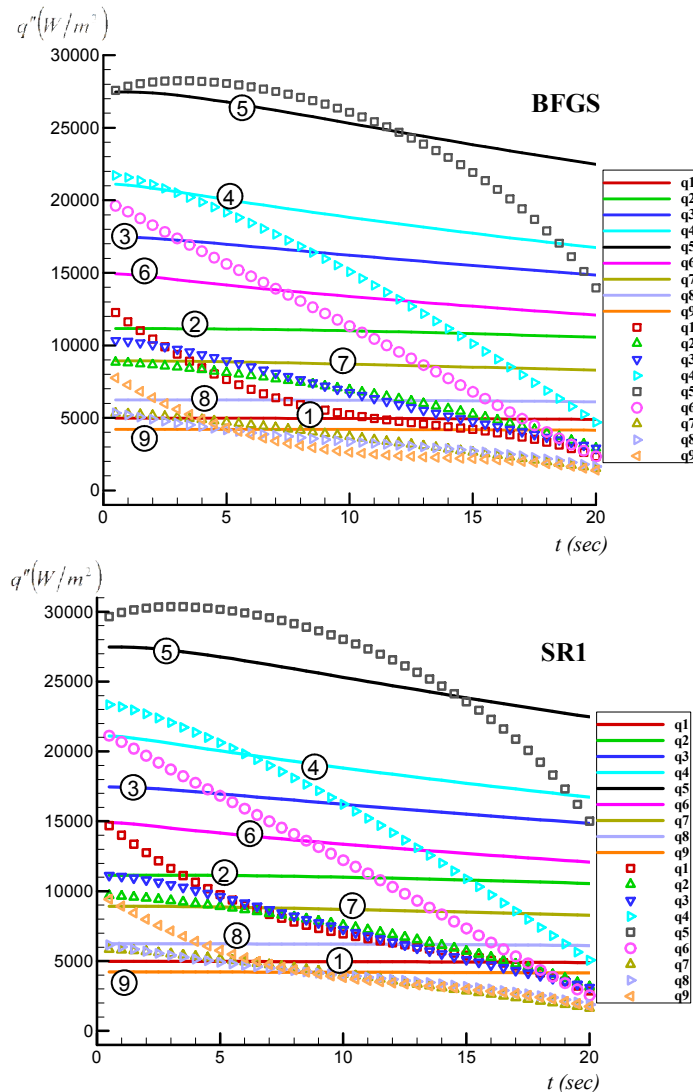


Figure 11: Heat fluxes estimated by IHCP method versus those predicted by flow simulation in ANSYS

## 8 Conclusions

In this paper, the VMM is used to compute the surface heat flux in an empirical inverse heat conduction problem (IHCP). The SR1 formula shows to be able to reduce the objective function a little faster than the BFGS formula. It is found to apply a high value for  $\sigma_t$  is required in the ANSYS software for turbulent air flow in turbine blade cascade. Two conclusions also are drawn from this study which are very likely to be helpful in setting up a real IHCP application: (1) The effect of the temperature distribution inside the solid geometry at the start of the experiment on the IHCP results is significant specially in whole domain methods. In most of theoretical IHCP studies, a uniform or a known temperature distribution can be considered as the initial condition of the heat equation. However, there are a number of real engineering applications in which this temperature has a complex distribution inside the body, and its accurate determination is required. This may itself be burdensome such that separate accurate numerical modeling of the experiment is needed to resolve

temperature field within the body. (2) The second issue is related to the selection of installation locations of thermocouples. Theoretically, the most accurate estimations in an IHCP method are achieved if the temperature history of the points located at the active surface is available. Nevertheless, at least when the aim is the finding of “convective heat transfer” in a practical engineering problem, it is better not to install the tip of the sensor on the interface between solid and fluid in order to capture the solid temperature of the active surface. When the temperature gradient in the thermal boundary layer is high due to the high value of surface heat flux, and the sensor tip has been laid even a little inside the fluid within practical installation tolerances, the thermocouple is affected by the neighboring fluid temperature, and a considerable difference will exist between the sensor data and the desired temperature of the body surface. If the sensor tip is laid completely within the body but tangent to the surface, a part of the tip area does not have contact with the solid and the tip of thermocouple again may not sense exactly the solid temperature. Therefore, it is better to install the thermocouple inside the solid but very near to the active surface such that the solid completely covers the tip of the thermocouple.

There are some ideas in the outlook as future improvements and potentials of research in the subject of this work. These include the effect of using more accurate CFD techniques like quadratic grid system instead unstructured triangular grid in the boundary layer on the results of heat flux, a wider variety of case studies such as studies of ranges of Biot, Fourier, and Nusselt numbers. The future work shall include the application of a higher resolution of the temperature measuring points and heat flux components. It is also suggested to try thermocouples which have wires with the minimum possible diameter. This is because the geometry equipped with grooves of thermocouple produces error and deviation from the original model. Using Infra Red Thermography methods for temperature measurements on the surface of the body along with the proposed method would likely yield more accurate estimations than those acquired from using classical thermocouples. One method is InfraRed cameras that can provide higher resolution of temperature measurements on the body surface. Nonetheless, Infra Red cameras are not possible in some applications. For example, the use of this technique does not seem applicable for measuring of temperature of a running turbomachinery blade in working conditions, or for point 3 in Figure 4 while the blades are mounted in the cascade as that point is invisible for camera.

## Acknowledgement

The authors gratefully acknowledge the financial support of the Alexander von Humboldt Foundation for the scholarship that made this study possible.

## References

- Alifanov O.M.: *Inverse Heat Transfer Problems*, Springer-Verlag, Berlin (1994).
- Ames F.E., Experimental study of vane heat transfer and aerodynamics at elevated levels of turbulence, NASA CR 4633,(1994).
- Byvaltsev P.M. and Nagashima T.: Correlation for numerical and experimental heat transfer data at the turbine blade surface, *JSME International Journal Series B*, 41, 1, (1998), 191-199.
- Butler R.J., Byerley A.R., Van Treuren K., and Baughn J.W.: The effect of turbulence intensity and length scale on low-pressure turbine blade aerodynamics, *International Journal of Heat and Fluid Flow*, 22, (2001), 123-133.
- Chen W.L. and Yang Y.C., On the inverse heat convection problem of the flow over a cascade of rectangular blades, *International Journal of Heat and Mass Transfer*, 51, (2008), 4184–4194.

- Choi J., Teng S., Han J.C., and Ladeinde F.: Effect of free-stream turbulence on turbine blade heat transfer and pressure coefficients in low Reynolds number flows, *International Journal of Heat and Mass Transfer*, 47, (2004), 3441–3452.
- Das M.K., Tariq A., Panigrahi P. K., and Muralidhar K., Estimation of convective heat transfer coefficient from transient liquid crystal data using an inverse technique, *Inverse Problems in Science and Engineering*, 13, 2, (2005), 133-155.
- Gardarein J.L., Corre Y., Rigollet F., Le Niliot C., Reichle R. and Andrew P.: Thermal quadrupoles approach for two-dimensional heat flux estimation using infrared and thermocouple measurements on the JET tokamak, *International Journal of Thermal Sciences*, 48, 1, (2009), 1-13.
- Heng Y., Mhamdi A., Wagner E., Stephan P., and Marquardt W.: Estimation of local nucleate boiling heat flux using a three-dimensional transient heat conduction model, *Inverse Problems in Science and Engineering*, 18, 2, (2010), 279-294.
- Huang C.H., Jan L. C., Li R. and Shih A.J.: A three-dimensional inverse problem in estimating the applied heat flux of a titanium drilling – Theoretical and experimental studies, *International Journal of Heat and Mass Transfer*, 50, (2007), 3265-3277.
- Kassab A.J., Divo E., and Kapat J.S.: Multi-dimensional heat flux reconstruction using narrow-band thermochromic liquid crystal thermography, *Inverse Problems in Engineering*, 9, 5, (2001), 537-559.
- Kowsary F., Behbahaninia A., and Pourshaghaghay A.: Transient heat flux function estimation utilizing the Variable Metric Method, *International Communications in Heat and Mass Transfer*, 33, 6, (2006), 800-810.
- Lukšan L. and Spedicato E.: Variable metric methods for unconstrained optimization and nonlinear least squares, *Journal of Computational and Applied Mathematics*, 124,(2000), 61-95.
- Louahlia-Gualous H., Baonga J. B.: Experimental Study of Unsteady Local Heat Transfer for Impinging Miniature Jet, *Heat Transfer Engineering*, 29, 9, (2008), 782-792.
- Manual of ANSYS 12.
- Nallathambi A. K. and Specht E.: Estimation of heat flux in array of jets quenching using experimental and inverse finite element method, *Journal of Materials Processing Technology*, 209, (2009), 5325-5332.
- Özisik M.N., and Orlande H.R.B.: *Inverse Heat Transfer*, Taylor & Francis, New York (2000).
- Pourshaghaghay A., Kowsary F., and Behbahaninia A.: Comparison of four different versions of the Variable Metric Method for solving inverse heat conduction problems, *Heat and Mass Transfer*, 43, 3, (2007), 285-294.

---

*Address:* Institute of Turbomachinery and Fluid Dynamics (TFD),  
 Leibniz Universität Hannover, Hannover, Germany  
 email: [seume@tfd.uni-hannover.de](mailto:seume@tfd.uni-hannover.de), Corresponding Author: [apoursh@gmail.com](mailto:apoursh@gmail.com)